PROCEEDINGS OF SCIENCE

Particle acceleration in core-collapse supernova remnant expanding inside the wind bubble

Samata Das,[a,b] **Robert Brose,**[c] **Martin Pohl,**[a,b,*] **Dominique M.-A. Meyer**[b] **and Iurii Sushch**[d,e]

[a] *DESY, Platanenallee 6, Zeuthen D-15738 , Germany*
[b] *University of Potsdam, Institute of Physics and Astronomy, Karl-Liebknecht-Strasse 24/25, Potsdam 14476, Germany*
[c] *Dublin Institute for Advanced Studies, 31 Fitzwilliam Place, Dublin 2, Ireland*
[d] *North-West University, Centre for Space Research, Potchefstroom 2520, South Africa*
[e] *Astronomical Observatory of Ivan Franko National University of L'viv, vul. Kyryla i Methodia 8, L'viv 79005, Ukraine*

E-mail: marpohl@uni-potsdam.de

The complex environments around core-collapse supernova remnants (SNRs) originates from their massive progenitors and shapes the spectra and morphology of non-thermal emissions from the remnants. We study the effects of the flow profiles and the magnetic field of the circumstellar medium on particle acceleration and emission from remnants and estimate the contribution of core-collapse SNRs to the Galactic CR production depending on progenitor masses.
We use *RATPaC* and *PLUTO* to simultaneously solve with spherical symmetry the hydrodynamic equations, the transport equations for CRs and scattering magnetic turbulence, and the induction equation for the large-scale magnetic field.
Our study shows a significant impact of the hot wind material. For example, the hot shocked wind created by 60 $M_\odot$ Wolf-Rayet progenitor significantly reduces the sonic Mach number of that SNR shock and hence persistently softens the particle spectra with spectral index $\sim$ 2.5, specifically at lower energy, and likewise the radio spectra with spectral index $\alpha \sim 0.8$ (energy flux, $S_\nu \propto \nu^{-\alpha}$). In contrast, the SNR with 20 $M_\odot$ Red-Super giant (RSG) progenitor produces soft radio spectra with spectral index $\sim$ 2.2, and correspondingly soft pion-decay gamma-ray spectra, only briefly during the interaction of the SNR shock with the dense RSG shell. For old remnants with shocks inside the shocked interstellar medium, we find soft pion-decay emission for all progenitors, consistent with the observed gamma-ray emission from SNRs like IC443, W44, G39.2¬0.3, etc.
The flux of CRs released into the interstellar medium is the highest for low-mass progenitors that are in the RSG phase in the pre-supernova stage. The total production spectrum of cosmic rays injected into the interstellar medium from remnants with 35 $M_\odot$ progenitor has a spectral index of $s \sim 2.4$ at higher energies which is comparable with the spectra predicted by Galactic propagation models.

38th International Cosmic Ray Conference (ICRC2023)
26 July - 3 August, 2023
Nagoya, Japan

*Speaker

PoS(ICRC2023)615

1. Introduction

Massive stars ($M_\star > 8M_\odot$) structure their circumstellar medium (CSM) through ionizing radiation and stellar winds during different evolutionary stages. Therefore, when massive stars explode as core-collapse supernova remnants (SNRs), the generated SNR blast waves will expand inside the complex wind-blown bubbles, and consequently, the dynamics of SNRs should be regulated by the CSM parameters [1].

SNRs are considered to be major sources of galactic cosmic rays (CRs) that are accelerated by the Diffusive Shock Acceleration (DSA) process at SNR shocks. In the core-collapse scenario, particle acceleration and emission from remnants should be affected by the interactions between SNRs and respective wind-blown bubbles. In our previous study [2], the spectral evolution and emission morphology of core-collapse SNRs were extensively studied using simulated CSM for the stellar track of a 60 $M_\odot$ star and considering Bohm-like diffusion for energetic particles. Apart from the shape of the wind bubbles, the self-generated magnetic field amplification can also influence the spectra of accelerated particles, specifically during later times of evolution [3]. Therefore, the core-collapse SNRs inside wind bubbles should be explored by the combined effect of the CSM and the CR-streaming instabilities along with their impact on CR diffusion as described in our most recent study (Das et al. 2023, submitted). In this context, we have investigated the following aspects here:

a. Effects on the spectra of accelerated particles of the different wind bubbles around progenitors with different Zero Age Main Sequence (ZAMS) masses.

b. The reduction in the driving of scattering magnetic turbulence on account of the escape of high-energy particles from the remnants, and the subsequent softening of particle spectra at higher energies for older remnants.

c. The spectra of the total CR production at SNRs as a function of the progenitor mass.

d. The temporal evolution of the non-thermal emission spectra as well as the SNR morphology during the expansion of remnants through different regions of the wind bubble.

2. Numerical modeling

The diffusive shock acceleration at SNR forward shock has been modelled in test-particle approximation using RATPaC (Radiation Acceleration Transport Parallel Code) [4].

2.1 Hydrodynamics

The Euler hydrodynamic equations including an energy source-sink term, considering the magnetic field as dynamically unimportant, can be described as :

$$\frac{\partial}{\partial t}\begin{pmatrix}\rho\\ \mathbf{m}\\ E\end{pmatrix} + \nabla\begin{pmatrix}\rho\mathbf{u}\\ \mathbf{m}\mathbf{u}+P\mathbf{I}\\ (E+P)\mathbf{u}\end{pmatrix}^T = \begin{pmatrix}0\\ 0\\ S\end{pmatrix} \tag{1}$$

$$\frac{\rho\mathbf{u}^2}{2} + \frac{P}{\gamma-1} = E; \quad \gamma = \frac{5}{3} \tag{2}$$

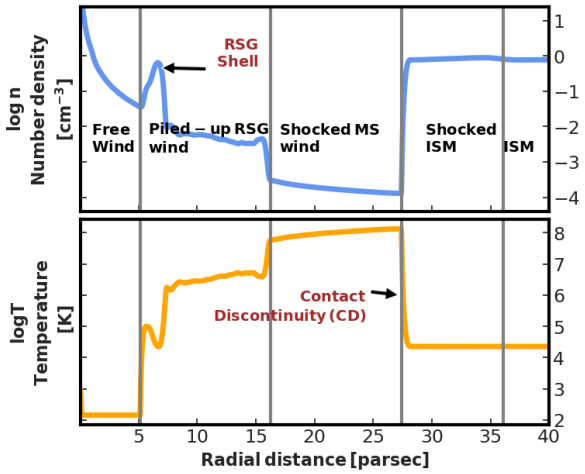

Figure 1: Pre-supernova CSM profiles of the number density, n, in the upper panel and the temperature, T, in the lower panel for the $20\,M_\odot$ **progenitor.** Vertical grey lines mark the boundaries of specific regions: free red supergiant (RSG) stellar wind (region 1), piled-up RSG wind (region 2), shocked main sequence (MS) wind (region 3), shocked interstellar medium (ISM) (region 4), and ISM (region 5). The RSG shell indicates the accumulation of RSG wind, $R_{\rm RSG}$ denotes the transition between RSG and MS wind, and CD represents the contact discontinuity between shocked wind and ISM.

where ρ, **u**, **m**, P, E, S are the mass density, flow velocity, momentum density, thermal pressure, total energy density, and source-sink term which includes the optically-thin cooling and radiative heating for the construction of CSM at the pre-supernova stage, respectively. **I** is the unit tensor.

- **Construction of CSM at pre-supernova stage**: The structure of CSM at the pre-supernova stage is obtained by performing hydrodynamic simulation in 1-D spherical symmetry using PLUTO code [5] for the entire lifetime of massive progenitor stars. The stellar wind properties are taken from the pre-calculated stellar evolutionary tracks, [6] for $20\,M_\odot$, and $35\,M_\odot$ stars and [7] for $60\,M_\odot$ star. As an example of simulated CSM structure, Figure 1 illustrates the flow profiles of the wind bubble around a $20\,M_\odot$ progenitor star at the pre-supernova stage, after around 8.64 million years.

- **Introducing supernova explosion**: Supernova explosions have been introduced through the insertion of appropriate supernova ejecta profiles, for example, the ejecta mass for SNRs from $20\,M_\odot$, $35\,M_\odot$, and $60\,M_\odot$ progenitors are $3.25\,M_\odot$, $7.75\,M_\odot$ and $11.75\,M_\odot$, respectively, in the corresponding pre-supernova stage CSM, described in [2] and Das et al. 2023 (submitted).

2.2 Magnetic field

The total magnetic field strength in the entire system is given by

$$B_{\rm tot} = \sqrt{B_0^2 + B_{\rm turb}^2}\,, \tag{3}$$

where B_0 and $B_{\rm turb}$ are the large-scale and turbulent magnetic field, respectively.

2.2.1 Large-scale magnetic field

Simulating the CSM magnetic field for the lifetime of progenitor stars by solving magneto-hydrodynamic (MHD) equations is out of scope. We parametrise the CSM magnetic field for different stars using the information about the stellar magnetic field and magnetic flux conservation [2]. For instance, the $20\,M_\odot$ star becomes a red supergiant (RSG) at the pre-supernova stage and, considering a weak surface field of $1 - 10\,$G [8], the magnetic field in the free wind region is set

up as a Parker spiral with predominantly toroidal magnetic field. The CSM magnetic field for this $20 M_\odot$ star can be written as,

$$B_{0,\,20\,\mathrm{M}_\odot} = \begin{cases} (1.07\ \mu\mathrm{G})\frac{R_{\mathrm{RSG}}}{r} & \text{regions 1 \& 2} \\ 0.35\ \mu\mathrm{G} & \text{region 3} \\ 4.68\ \mu\mathrm{G} & \text{region 4} \\ 4.0\ \mu\mathrm{G} & \text{region 5 .} \end{cases} \tag{4}$$

where at $R_{\mathrm{RSG}} = 16.3\,\mathrm{pc}$ the RSG wind transitions to the MS wind (cf. Figure 1). The subsequent evolution of the large-scale magnetic field is determined by passive transport in the gas flow and is given by the induction equation in 1-D spherical symmetry,

$$\frac{\partial \mathbf{B_0}}{\partial t} = \nabla \times (\mathbf{u} \times \mathbf{B_0})\ . \tag{5}$$

This method mimics MHD for negligible magnetic pressure.

2.2.2 Magnetic turbulence

The temporal and spatial evolution of the magnetic turbulence spectrum can be described by a continuity equation for magnetic spectral energy density per logarithmic bandwidth, $E_w(r, k, t)$ [3],

$$\frac{\partial E_w}{\partial t} = -\nabla \cdot (\mathbf{u} E_w) - k\frac{\partial}{\partial k}(k^2 D_k \frac{\partial}{\partial k}\frac{E_w}{k^3}) + 2(\Gamma_g - \Gamma_d)E_w \tag{6}$$

where k refers to the wavenumber, D_k is the diffusion coefficient in wavenumber space describing cascading, and Γ_g, Γ_d are growth and damping rates, respectively. This transport equation for the magnetic turbulence spectrum has been solved in 1-D spherical symmetry, considering Alfvén waves as scattering centres for CRs. The non-resonant CR streaming instabilities are considered the dominant way of magnetic field amplification when the SNR shock is relatively fast and at later times, resonant modes give efficient amplification. But considering the non-resonant modes is beyond the scope of this study and therefore, we enhance the growth term for the resonant streaming instability by factor 10 [9] during the entire lifetime of the SNR as a simple proxy to get efficient amplification.

2.2.3 Diffusion coefficient

Alfvén waves as the scattering centres for CRs give the resonance condition, $k_{\mathrm{res}} = \frac{|q|\,B_0}{pc}$, where k_{res} is the resonant wavenumber, and q is the particle charge. Therefore, the diffusion coefficient coupled to E_w reads [3],

$$D_{\mathrm{r}} = \frac{4v}{3\pi} r_g \frac{U_B}{E_w} \tag{7}$$

where U_B is the energy density of the large-scale magnetic field and r_g represents the gyro-radius of particles in B_{tot}.

2.3 Particle acceleration

The time-dependent transport equation for the differential number density, N, of CRs

$$\frac{\partial N}{\partial t} = \nabla(D_{\rm r}\nabla N - \mathbf{u}N) - \frac{\partial}{\partial p}\left(\dot{p}N - \frac{\nabla.\mathbf{u}}{3}Np\right) + Q \tag{8}$$

have been solved in 1D spherical symmetry in a shock-centred co-ordinate system considering only DSA at the forward shock in test-particle limit, where $D_{\rm r}$ is the spatial diffusion coefficient, $\dot{p}$ corresponds to energy loss rate, and Q refer to the plasma velocity and the source term, respectively. The source term is defined as,

$$Q = \eta n_{\rm u}(V_{\rm sh} - V_{\rm u})\delta(R - R_{\rm sh})\delta(p - p_{\rm inj}) \tag{9}$$

where η is the injection efficiency, $n_{\rm u}$ and $V_{\rm u}$ are the upstream plasma number density and velocity, respectively, $V_{\rm sh}$ and $R_{\rm sh}$ are shock velocity and radius, respectively, and $p_{\rm inj}$ represents the momentum of injected particles.
The equations for the hydrodynamic evolution of SNR, the evolution of the large-scale magnetic field, and the CR and magnetic turbulence transport equation have been solved in parallel using RATPaC.

3. Results

3.1 Shock parameters

The speed of the forward shock of SNRs with different progenitors depends on the characteristics of the wind bubbles through which the forward shock expands. The sub-shock compression ratio ($R_{\rm sub}$) depends on the sonic Mach number ($M_{\rm s}$), following $R_{\rm sub} = (1+\gamma)M_{\rm s}/((1-\gamma)M_{\rm s}+2)$. The evolution of forward shock parameters was described elaborately for SNRs with different progenitor masses in [2] and Das et al. 2023 (submitted). The most important feature is that $R_{\rm sub}$ reaches 1.5 for SNRs with very massive progenitors that have a very fast wind, for example, the propagation of SNR through the hot shocked wind region created by 60 $M_\odot$ star persistently reduces $R_{\rm sub}$ from value 4 for strong shock.

3.2 Particle acceleration

In the core-collapse scenario, the resulting particle spectra are affected both by the complex hydrodynamics of the corresponding wind bubbles and by the dynamics of the self-consistent turbulence. Additionally, the profiles of large-scale magnetic fields, deriving from the passive transport of field strength in CSM can also have impacts on particle acceleration [10].
In our time-dependent treatment of the transport of CRs and Alfvénic turbulence, the driving of turbulence diminishes, because the CR gradient decreases at later stages of SNR evolution [11]. Consequently, the acceleration timescale increase and particles at higher energy may escape from the shock vicinity. Therefore, the downstream particle spectra become softened above a certain energy (Das et al. 2023, submitted). Here, we only mention a comparative analysis of the total production spectra of protons, including particles outside of SNRs considering remnants with progenitors having different ZAMS masses, shown in Figure 2.

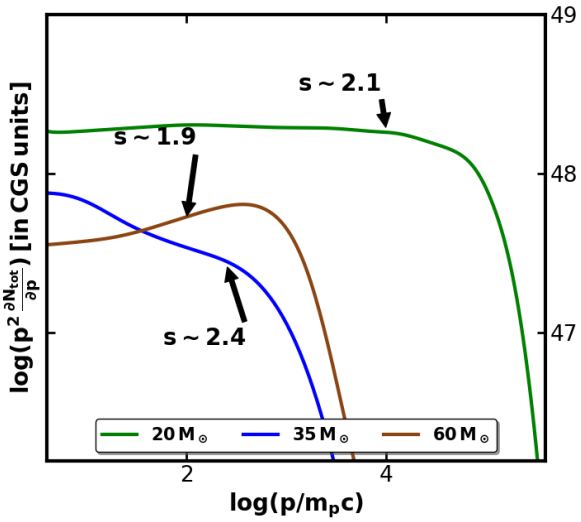

Figure 2: Proton number spectra injected into ISM by SNRs for different ZAMS masses of the progenitor. Volume-integrated spectra of all accelerated protons residing downstream and upstream of the SNR forward shock at the end of the lifetime of SNRs with 20 $M_\odot$, 35 $M_\odot$ and 60 $M_\odot$ progenitors. At this stage, the size and age of remnants are 32 pc and 25000 yrs for 20 $M_\odot$, 52 pc and 30000 yrs, and 90pc and 90000 yrs for 35 $\odot$ and 60 $\odot$ progenitors, respectively.

Progenitors with 20 $M_\odot$, 35 $M_\odot$, 60 $M_\odot$ ZAMS masses evolve through MS, RSG stages and MS, RSG, Wolf-Rayet (WR) stages, and MS, RSG, Luminous Blue Variable (LBV) stages. Therefore, the hydrodynamics and magnetic field strength of respective wind bubbles will be distinct which shape particle spectra with different spectral features. Besides these, the flux of injected particles into ISM at certain energies by different SNRs depends on the density of the plasma that the shock passes through, as well as the size of the remnant. As the wind bubble from 20 $M_\odot$ star comprises denser RSG wind and becomes RSG at the pre-supernova stage, the resulting injected spectra into ISM are prominent in comparison to that from the other two remnants. Further, the cut-off energy of injected spectra is also different depending on SNR shock velocity, magnetic field strength and the size of the remnant. Figure 2 also depicts the different spectral indices of proton production spectra at higher energies and the softest spectrum comes from the SNR with 35 $M_\odot$ star with spectral index of $s = 2.4$ which fits with the required spectral shape of CRs released into ISM predicted by Galactic propagation models.

3.3 Non-thermal emission

The processes of non-thermal emission from the remnants include synchrotron emission, inverse Compton scattering considering only the cosmic microwave background photon field, and the decay of neutral pions. In this article, we only highlight the radiation from the SNR of the 20 $M_\odot$ star to provide a glimpse of the time-dependent evolution of emission.

Synchrotron and gamma-ray emission flux in Figures 3 and 4, respectively suggest the entire non-thermal emission originated in the interior of the remnant below the age of about 5000 years. At the early stages of evolution, the SNR interact with a strong magnetic field in the free wind region which leads to the highest X-ray flux at this stage, shown at 500 years. While the SNR collides with RSG shell, shown in Figure 1, between 750 years and 1600 years, the radio spectra start to soften to a spectral index of $\alpha \approx 0.54$ ($S_\nu \propto \nu^{-\alpha}$) and the spectral index of pion-decay emission reaches 2.2. This stage of remnant evolution may be comparable to Cas A, and although the progenitor of Cas A may differ from the 20 $M_\odot$ star, the spectral index for accelerated protons obtained in our study is comparable with that estimated by [12]. Later on, during the forward-shock passage

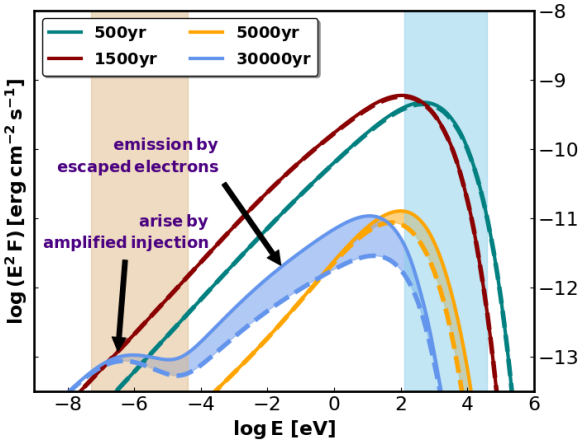

Figure 3: Synchrotron emission from the SNR at different ages for the $20\,M_\odot$ **progenitor.** The upper boundaries of the shaded regions indicate the total emission from the remnant whether the lower ones denote emission from the downstream of SNR forward shock. The brown band indicates the 50 MHz − 10 GHz range and the blue band denotes 0.1 keV − 40 keV.

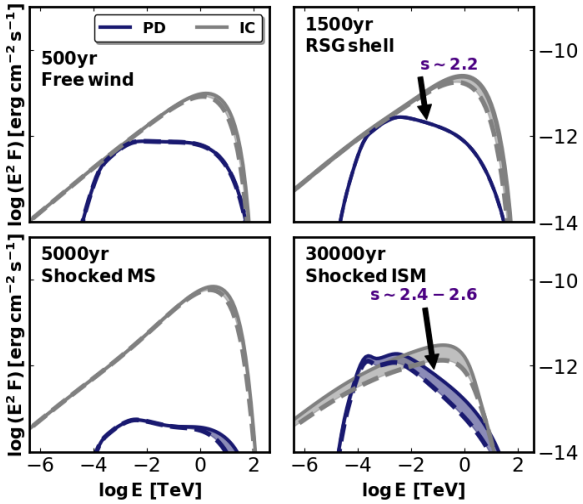

Figure 4: Gamma-ray emission by pion-decay (PD) and inverse Compton (IC) scattering at different ages for the $20\,M_\odot$ **star.** The boundaries of the shaded regions indicate the total emission and that from the interior.

through the shocked ISM, a significant fraction of the synchrotron flux is produced in the upstream region, depicted at 30000 years as well as a fraction of the gamma-ray emission on account of particle escape. The spectral index for pion-decay emission reaches 2.4 − 2.6 and this kind of soft gamma-ray spectra are observed from SNRs for example IC443, W44, G 39.2 − 0.3, etc., that are expanding in or near the dense molecular clouds [13]. The morphology of the remnant in other wave bandss also evolves time-dependently.

4. Conclusions

In this work, considering SNRs with progenitors of different ZAMS masses we have time-dependently calculated spectra of accelerated particles by using self-consistent magnetic turbulence. It can be concluded that

- The spectral shape depends on the flow profile and magnetic field of the wind bubble along with the CR-driven magnetic turbulence. Therefore, the spectra of particles released into the ISM from remnants with different progenitors should vary and demonstrate different spectral softness at higher energies.

- From the considered SNRs, dominating flux of particles is injected into ISM from the lower massive star because of the presence of RSG phase during the pre-supernova stage.
- The non-thermal emissions from the core-collapse remnant depend on the region where the SNR shock resides and hence, changes time-dependently. Further, emissions from the escaped particles around the remnants are also obtained in this study.

References

[1] R.A. Chevalier and E.P. Liang, *The Interaction of Supernovae with Circumstellar Bubbles*, *ApJ* **344** (1989) 332.

[2] S. Das, R. Brose, D.M.A. Meyer, M. Pohl, I. Sushch and P. Plotko, *Spectral softening in core-collapse supernova remnant expanding inside wind-blown bubble*, *A&A* **661** (2022) A128 [2203.03369].

[3] R. Brose, I. Telezhinsky and M. Pohl, *Transport of magnetic turbulence in supernova remnants*, *A&A* **593** (2016) A20 [1606.04477].

[4] I. Telezhinsky, V.V. Dwarkadas and M. Pohl, *Particle spectra from acceleration at forward and reverse shocks of young Type Ia Supernova Remnants*, *Astroparticle Physics* **35** (2012) 300 [1110.0361].

[5] A. Mignone, G. Bodo, S. Massaglia, T. Matsakos, O. Tesileanu, C. Zanni et al., *PLUTO: A Numerical Code for Computational Astrophysics*, *ApJs* **170** (2007) 228 [astro-ph/0701854].

[6] S. Ekström, C. Georgy, P. Eggenberger, G. Meynet, N. Mowlavi, A. Wyttenbach et al., *Grids of stellar models with rotation. I. Models from 0.8 to 120 $M_\odot$ at solar metallicity ($Z = 0.014$)*, *A&A* **537** (2012) A146 [1110.5049].

[7] J.H. Groh, G. Meynet, S. Ekström and C. Georgy, *The evolution of massive stars and their spectra. I. A non-rotating 60 $M_\odot$ star from the zero-age main sequence to the pre-supernova stage*, *A&A* **564** (2014) A30 [1401.7322].

[8] B. Tessore, A. Lèbre, J. Morin, P. Mathias, E. Josselin and M. Aurière, *Measuring surface magnetic fields of red supergiant stars*, *A&A* **603** (2017) A129 [1704.07761].

[9] R. Brose, M. Pohl and I. Sushch, *Morphology of supernova remnants and their halos*, *A&A* **654** (2021) A139 [2108.10773].

[10] I. Sushch, R. Brose, M. Pohl, P. Plotko and S. Das, *Leptonic Nonthermal Emission from Supernova Remnants Evolving in the Circumstellar Magnetic Field*, *ApJ* **926** (2022) 140 [2111.06946].

[11] R. Brose, M. Pohl, I. Sushch, O. Petruk and T. Kuzyo, *Cosmic-ray acceleration and escape from post-adiabatic supernova remnants*, *A&A* **634** (2020) A59 [1909.08484].

[12] L. Saha, T. Ergin, P. Majumdar, M. Bozkurt and E.N. Ercan, *Origin of gamma-ray emission in the shell of Cassiopeia A*, *A&A* **563** (2014) A88 [1401.5626].

[13] M. Cardillo, M. Tavani, A. Giuliani, S. Yoshiike, H. Sano, T. Fukuda et al., *The supernova remnant W44: Confirmations and challenges for cosmic-ray acceleration*, *A&A* **565** (2014) A74 [1403.1250].

PoS(ICRC2023)615